Signal Amplification *via* Biological Self-Assembly of Surface-Engineered Quantum Dots for Multiplexed Subattomolar Immunoassays and Apoptosis Imaging

Joonhyuck Park,[†] Youngrong Park,[‡] and Sungjee Kim[†,‡,*]

[†]School of Interdisciplinary Bioscience and Bioengineering, and [‡]Department of Chemistry, Pohang University of Science and Technology (POSTECH), San 31, Hyoja-Dong, Nam-Gu, Pohang, Gyeong-Buk, South Korea 790-784

ABSTRACT The parallel and highly sensitive detection of biomolecules is of paramount importance to understand biological functions at the single cell level and for various medical diagnoses. Surface-engineered semiconductor quantum dots (QDs) have been demonstrated to act as a signal amplifiable reporter in immunoassays. This takes advantage of the QDs' robustness against self-quenching in proximity and the tunability of their surface properties. A streptavidin (SA) and biotin QD conjugate pair containing a zwitterionic surface modification was designed for QD self-assembly with minimal nonspecific adsorption. Typical sandwich-type immunoassay procedures were adopted, and the targeted protein binding events were effectively transduced and amplified by the fluorescence of the SA—biotin QD conjugates. The detection limit of myoglobin in 100% serum was determined to be at the subattomolar (tens of copies per milliliter) level, which was achieved by using 100 cycles of the layer-by-layer QD assembly. Adsorption kinetics studies and Monte Carlo simulations revealed that this highly sensitive signal amplification was accomplished by the zwitterionic surface, which gave equilibrium constants 5 orders of magnitude larger for specific binding than for nonspecific binding. The QD conjugates showed an effective multivalency of two, which resulted in a broad linear dynamic range spanning 9 orders of magnitude of target protein concentrations. The assay can be highly miniaturized and multiplexed, and as a proof-of-concept, parallel and rapid detection of four different cancer markers has been successfully demonstrated. To demonstrate that this QD signal amplification can be a universal platform, sensitive imaging and early detection of apoptotic cells were also showcased.

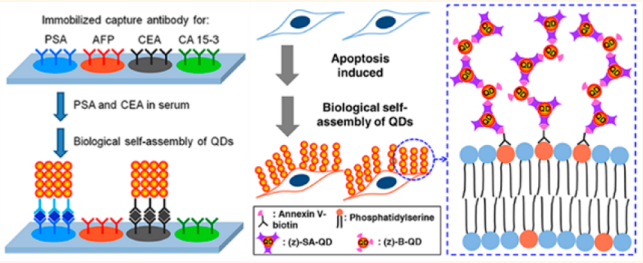

KEYWORDS: quantum dots · apoptosis imaging · immunoassay · self-assembly · signal amplification

Genomics and proteomics researchers have discovered many new biomarkers that have the potential to greatly improve the diagnosing, prognosing, and monitoring of cancers and other medical conditions.[1,2] A rapid and sensitive assay that detects multiple specific molecules from the complex mixture present in serum would allow for early intervention and the treatment and better management of diseases. Antibody-based recognition remains one of the most promising strategies for such applications. Immunoassays typically use reporters to transduce the antigen binding interactions into a quantifiable change. These reporters include radioactive tracers,[3] luminescent probes,[4] and substrates containing antibody-linked enzymes.[5] In the case of enzyme-linked immunosorbent assays (ELISA),[5] a target protein can be captured by an antibody and then sandwiched by a second antibody that incorporates a catalytic product-generating enzyme. Much attention has been focused on signal amplification without using enzymes.[6−8] DNA has been exploited as an amplifiable signal reporter in techniques such as immuno-PCR,[9] DNA-amplified electrochemical,[10] and liposome-PCR[11] assays without using a chromophore-generating enzyme. Metallic

* Address correspondence to sungjee@postech.ac.kr.

Received for review August 12, 2013 and accepted September 24, 2013.

Published online September 24, 2013
10.1021/nn4042078

nanoparticle catalysts have replaced the enzyme in ELISA in some studies.[12] Biobarcode-based "scanometric" assays allow for simple, chip-based detection and take advantage of antibody-associated gold nanoparticles that can catalyze the reduction of silver ions, which leads to a marked enhancement of the scattering signal.[13] Fluorescent signals can typically be several orders of magnitude more sensitive than colorimetric signals. Signal amplification through the deposition of fluorophores should provide a simple, chip-based detector with very high sensitivity. However, the deposition of conventional fluorescent dyes in close proximity would quickly result in self-quenching. For example, polymer-based multiple fluorophore probes have had limited success in immunoassays due to this quenching problem.[14] In addition, unlike the selective deposition of metal ions onto metallic nanoparticles, the selective deposition of fluorophores demands a new assembly strategy.

Semiconductor quantum dots (QDs) are bright nanoemitters that have demonstrated the potential for many applications, including biological probes for imaging and assays.[15−25] Here, we present QDs as a signal amplifiable reporter for immunoassays with high sensitivity and selectivity. The use of QDs for fluorescent signal amplification is advantageous because QDs do not easily self-quench when aggregated or assembled.[26] For example, Giorgio *et al.* have demonstrated subpicomolar protein detection using self-assembled agglomerations of QD−antibody conjugates in solution phase.[26,27] QDs can also provide multiple conjugation sites on the surface. A QD conjugated with streptavidin (SA) or biotin is designed to exploit the strong specific binding motif of SA and biotin for self-assembly. Specific assembly of QDs requires sophisticated controls to minimize nonspecific adsorption. QDs have an ideal architecture for this purpose because their optical and surface adsorption properties can be completely decoupled. The fluorophore part (semiconductor QD core) can be completely passivated inside while the outer surface can solely consist of an engineered layer. Zwitterionic surface modification of the QDs is used to overcome the problem of nonspecific adsorption. Using QDs that can biologically self-assemble with minimal nonspecific adsorption, target protein binding events can be effectively transduced and amplified by the assembled QD fluorescence. This biological self-assembly of QDs for signal amplification is free from the background signal problems, which is often observed in metallic nanoparticle-based electroless metal depositions of multiple rounds.[28] Our QD-amplified immunoassay demonstrated a subattomolar limit of detection for the targeted proteins (tens of copies per milliliter) and can also be highly miniaturized and multiplexed. To demonstrate the capability of the multiplexed immunoassay to detect different proteins, the parallel detection of four different cancer markers has been achieved. The sensitivity comparable to the conventional ELISA has been achieved in less than half the time needed for ELISA, without noticeable cross-reactivity. To demonstrate that this QD signal amplification can be a universal platform, sensitive imaging and early detection of apoptotic cells were also showcased.

RESULTS AND DISCUSSION

Characterization of QD Biological Self-Assembly onto Beads. We have recently developed the zwitterionic surface engineering of QDs. Zwitterionic QDs are compact with a surface ligand hydrodynamic thickness of less than 2 nm, forming stable colloids over a broad pH range and even in saturated NaCl solution, and show minimal nonspecific adsorption.[29] Others have reported similar colloidal properties for zwitterionic surface ligands on nanoparticles.[30−32] CdSe/CdZnS (core/shell) QDs and the zwitterionic surface ligand were synthesized as previously reported and used for the experiments herein.[29] We have performed careful experiments on QDs with mixed surface ligands. Remarkably, a partial surface coverage (for example, 50% homogeneous coverage) with the zwitterionic ligand can endow the QDs with a colloidal stability and resistance to nonspecific adsorption that are equivalent to complete zwitterionic surface coverage.[29] QDs can be co-decorated with the zwitterionic ligand and dihydrolipoic acid (DHLA), where the carboxylic acid in DHLA can be used for conjugation to streptavidins (SAs). The resultant zwitterion-decorated SA−QD conjugate (abbreviated as (z)-SA−QD) shows high specificity to biotin with minimal nonspecific adsorption. Similarly, a biotin−QD conjugate with zwitterionic decoration (abbreviated as (z)-B−QD) has been successfully obtained (Figure 1a). The number of conjugated SAs or biotins per QD was judiciously controlled by the mole ratio used for the reaction, which yielded an average of three SAs for (z)-SA−QD and 40 biotins for (z)-B−QD (see Supporting Information (SI) for the conjugation efficiency). The optical properties of (z)-SA−QD and (z)-B−QD remained unchanged after the conjugations; the photoluminescence (PL) quantum efficiency was ~30%, and the emission peak was centered at 610 nm (Figure S1). The high specificity between the SA−biotin motifs on the QDs can be guaranteed by the zwitterionic QD surface engineering because the zwitterionic surface minimizes nonspecific adsorption and facilitates the interactions between each SA and biotin by the small hydrodynamic size (Figure S2). The highly specific, layer-by-layer self-assembly of (z)-SA−QD and (z)-B−QD was first tested using biotinylated agar beads. Conjugates bearing surfaces decorated by sulfonate functional groups instead of the zwitterionic moieties, (s)-SA−QD and (s)-B−QD, were used as controls (Figure 1a). The sulfonate-bearing surface ligand was synthesized as previously reported.[33]

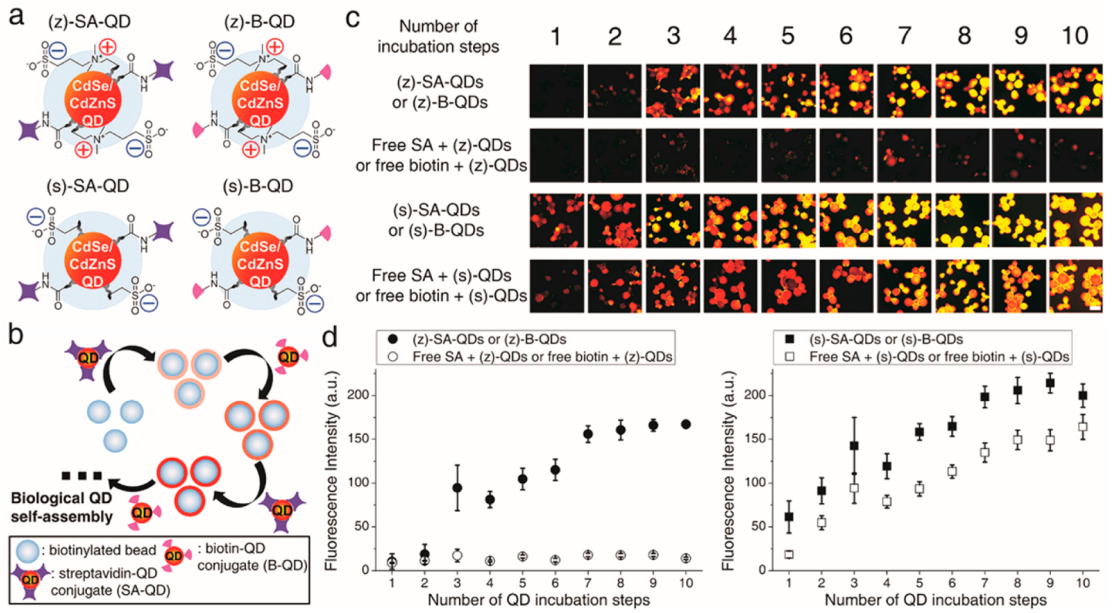

Figure 1. Streptavidin (SA) and biotin QD conjugate pair with a zwitterionic surface can self-assemble in a highly specific layer-by-layer fashion. (a) Schematic representations of QD conjugates with different surface decorations: SA−QD conjugate with zwitterionic surface (z)-SA−QD, biotin−QD conjugate with zwitterionic surface (z)-B−QD, SA−QD conjugate with sulfonate surface (s)-SA−QD, and biotin−QD conjugate with sulfonate surface (s)-B−QD. (b) Schematic for biological QD self-assembly onto biotinylated agar beads. (c) Fluorescent microscope images of the beads after each QD assembly incubation step from 1 to 10 with the (z)-SA−QD/(z)-B−QD pair on the first row, physical mixture of free SAs (or biotins) and unconjugated (z)-QDs on the second row, sulfonate surface-decorated SA−QD/biotin−QD conjugates, (s)-SA−QD/(s)-B−QD pair on the third row, and physical mixture of free SAs (or biotins) and unconjugated (s)-QDs on the fourth row (scale bar: 100 μm). (d) Plots of the bead fluorescence intensities *vs* number of QD incubation steps for the (z)-SA−QD/(z)-B−QD pair (closed circles in the left panel), physical mixture of free SAs (or biotins) and unconjugated (z)-QDs (open circles in the left panel), the sulfonate surface-decorated SA−QD/biotin−QD conjugates, (s)-SA−QD/(s)-B−QD pair (closed squares in the right panel), and physical mixture of free SAs (or biotins) and unconjugated (s)-QDs (open squares in the right panel).

The biotinylated agar beads were first incubated with the (z)-SA−QDs in a phosphate buffer solution (PBS), and the beads were collected and washed before the second incubation with (z)-B−QD PBS solution. The beads were incubated for 5 min each in the QD solutions, and water rinse took 20 s each. After the beads were washed again, the incubation was repeated by alternation of (z)-SA−QD and (z)-B−QD (Figure 1b). Each incubation cycle has two sequential incubation steps with SA−QDs and B−QDs. As the incubation cycles were repeated, (z)-SA−QDs and (z)-B−QDs assembled layer-by-layer onto the beads, which continually increased in fluorescence intensity (first row in Figure 1c). A physical mixture of free SAs (or free biotin) and unconjugated zwitterionic QDs ((z)-QDs) was coincubated as an unconjugated control (second row in Figure 1c). (s)-SA−QD and (s)-B−QD conjugates were incubated using a procedure identical to that for (z)-SA−QD and (z)-B−QD (third row in Figure 1c). Unconjugated control experiments were also performed using physical mixtures of free SAs (or free biotin) and unconjugated sulfonate surface QDs ((s)-QD) (fourth row in Figure 1c). Fluorescent microscope images of the beads were taken after each incubation step, and the fluorescence intensity (FI) was plotted for all four cases (Figure 1d). Both the (z)-SA−QD/(z)-B−QD and (s)-SA−QD/(s)-B−QD pairs showed increasing FI with repeated incubation steps, which indicates the layer-by-layer assembly of the QDs *via* the SA and biotin binding. The (s)-SA−QD/(s)-B−QD pair showed slightly higher FI over the (z)-SA−QD/(z)-B−QD pair, presumably due to nonspecific adsorption. A similar study has reported QD layer-by-layer self-assembly using a SA and biotin binding motif for magnetic bead barcodes.[34] However, the unconjugated control experiments using physical mixtures showed a dramatic difference between the (z)-QD and (s)-QD cases. The physical mixture with the unconjugated (z)-QDs only marginally increased in FI over the repeated incubation steps, whereas the physical mixture with the unconjugated (s)-QDs exhibited a FI increase comparable to that of the SA/biotin conjugated QDs. This FI increase indicates a lower level of nonspecific adsorption for (z)-QDs than for (s)-QDs. When the FIs of the conjugated samples are subtracted from those of the unconjugated controls, only the zwitterionic surfaced QDs show meaningful selectivity for specific over nonspecific adsorption. This nonspecific adsorption accounts for the background signals in assay applications. The zwitterionic surface engineering of the QDs is essential for specificity of the QD signal amplification through self-assembly.

Myoglobin Immunoassay. The specific and stable amplification of fluorescence *via* the biological self-assembly

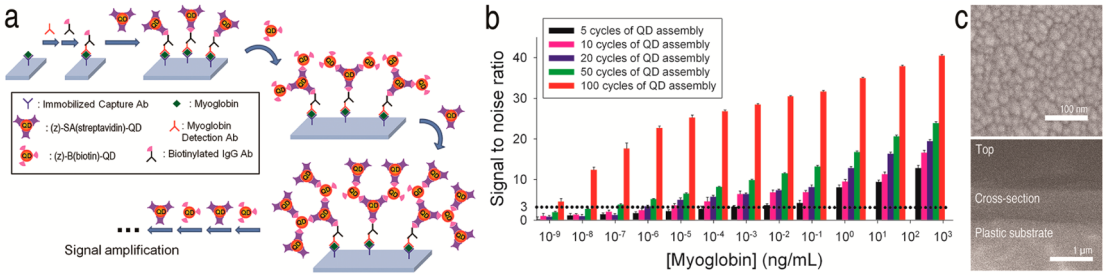

Figure 2. QD self-assembly-based signal amplification yields a subattomolar limit of detection for the myoglobin immunoassay. (a) Schematic of a myoglobin immunoassay using the (z)-SA−QD/(z)-B−QD pair for QD signal amplification by biological self-assembly. (b) Bar graph showing the QD fluorescence signal-to-noise ratios *vs* the concentration of myoglobin in 100% bovine calf serum after 5 (black), 10 (purple), 20 (blue), 50 (green), and 100 (red) QD assembly cycles. (c) Scanning electron microscopy images showing top (upper) and trans-sectional views (lower) of the assembled QD stacks on the substrate after 100 signal amplification cycles.

of QDs has been applied to immunoassays. As a proof-of-concept experiment, myoglobin immunoassay was performed using QDs as the signal amplifiable reporter. Myoglobin is released from damaged muscle tissue and is an important myocardial infarction marker.[35] This immunoassay followed the typical procedure for sandwich-type assays and used myoglobin samples in 100% bovine calf serum (BCS) (Figure 2a) to simulate complex media. Biotinylated secondary antibodies were attached to the antibody-sandwiched myoglobin (see Experimental Section for details) and alternatively treated with the (z)-SA−QD and (z)-B−QD conjugates to achieve layer-by-layer QD assembly from the biotinylated secondary antibodies. Using a mechanized dipper, the substrate was first dipped into a (z)-SA−QD solution (0.50 μM in PBS), rinsed in a DI water bath, and finally submerged in a (z)-B−QD solution (0.50 μM in PBS). Another rinsing step in the DI water bath completed one QD deposition cycle. The substrate was incubated for 5 min with each of the QD solutions, and each water rinse took 20 s. The myoglobin was diluted from 0.40 μg/mL to 0.98 ag/mL in 100% BCS. The QD assembly was cycled 5, 10, 20, 50, and 100 times, and the signal-to-noise ratio (SNR) of the fluorescence signals was obtained (Figure 2b and Figure S3 for raw data). The SNR is defined as the difference between the FI from myoglobin sample incubated area and that from the background (identical surfaces but myoglobin sample not incubated) divided by the standard deviation of the background FI. The SNRs increased with both the myoglobin concentration and the number of QD assembly cycles. After 100 cycles of QD assembly, the SNR was amplified enough to lower the limit of detection (LOD), defined by a SNR of greater than 3, to 0.98 ag/mL.[36] The volume of the myoglobin serum solution was 30 μL, and the LOD indicated that ~30 copies of myoglobin per milliliter could be detected, which is more than 10 million times more sensitive than conventional myoglobin ELISA (Figure S7).[37] Typically, fluoroscent immunosorbent assay (FIA) and chemiluminescent enzyme-linked immunosorbent assay (CLISA) are 10 to 100 times more sensitive than ELISA.[4,38] Our method is expected to be more than 100 000 times sensitive than conventional FIA or CLISA. Remarkably, as few as 5 QD assembly cycles achieved a LOD an order of magnitude smaller than that of conventional ELISA. This result proves that our layer-by-layer QD assembly signal amplification technique can provide a highly sensitive (tens of copies per milliliter) immunoassay after a reasonable length of time (17 h for the 100 cycle run). Alternatively, it can be exploited for rapid detection (less than 1 h for the 5 cycle run) with a LOD comparable to conventional tools (sub ng/mL). Our technique also showed a remarkably broad linear dynamic range (LDR) and exhibited an R^2 greater than 0.99 for a 9 order of magnitude concentration range, from 100 ag/mL to 400 ng/mL with sensitivity (Δ(signal)/Δlog[myoglobin]) of 7.1 (Figure S10). The sensitivity is more than 10 times larger than conventional myoglobin ELISA.[37] This LDR contrasts sharply with that of conventional ELISA (typically 25 to 250 ng/mL).[37] This wide LDR is well suited for simple and rapid quantifications that require neither dilution nor enrichment processes and suggests that the QDs rapidly form a flat layer and subsequently self-assemble by layer-by-layer stacking fashion. Both top and trans-sectional scanning electron microscopy (SEM) images of a substrate after 100 cycles of QD self-assembly are shown in Figure 2c. The top surface is flat and smooth with a domain size of ~10 nm. The trans-sectional image shows a ~610 nm thick assembled QD stack which can be ~150 layers of layer-by-layer-assembled QDs when close-packed assembly of dried state QDs is hypothesized. This massive stack explains the powerful amplification of the QD fluorescence signal. To investigate the effects of the serum media, the experiments were repeated using PBS instead of 100% BCS. The SNRs were only enhanced 15−20% compared to the BCS cases (Figure S4), which proves that our QD assembly-based signal amplification for immunoassay functions reasonably robust in complex media.

Kinetics Study and Monte Carlo Simulations on QD Assembly. To understand the underlying mechanisms behind the

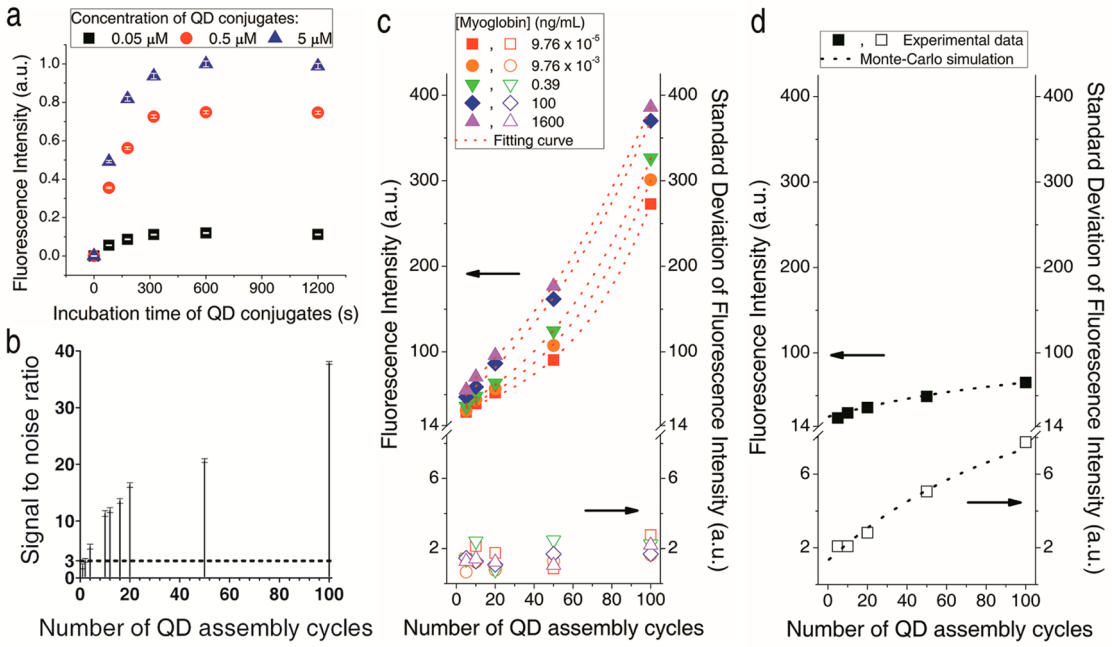

Figure 3. Adsorption kinetics and Monte Carlo simulation studies show a 5 order of magnitude difference between the specific and nonspecific binding equilibrium constants of the zwitterionic-modified QD conjugates. (a) Plots of the fluorescence intensity of QD conjugates on a myoglobin-captured (25 ng/mL) substrate *vs* the incubation time for four self-assembly cycles. The QD conjugate concentration was either 0.05 μM (black squares), 0.5 μM (red circles), or 5 μM (blue triangles). (b) Plots of the signal-to-noise ratio *vs* number of QD assembly cycles for myoglobin (25 ng/mL) in 100% bovine calf serum immunoassay. (c) Plots of the QD fluorescence intensity (filled symbols, scale on the left vertical axis) and standard deviation (empty symbols, scale on the right vertical axis) *vs* number of QD assembly cycles for myoglobin samples in 100% bovine calf serum with concentrations of 9.76 $\times$ 10^{-5}, 9.76 $\times$ 10^{-3}, 0.39, 100, and 1600 ng/mL (represented by the red squares, orange circles, green inverted triangles, blue diamonds, and magenta triangles, respectively). (d) Plots of the QD fluorescence intensity (filled squares, scale on the left vertical axis) and the standard deviation (empty squares, scale on the right vertical axis) *vs* number of QD assembly cycles for the background incubated in 100% bovine calf serum with no myoglobin. Dotted lines represent the results of the Monte Carlo simulations.

high sensitivity, speed, and broad LDR of immunoassays using QD self-assembly-based signal amplification, the assembly kinetics of both the signal and background were investigated along with different QD surfaces. The self-assembly of the (z)-SA−QD/(z)-B−QD pair was studied using 0.05, 0.5, and 5 μM concentrations, and the incubation time of the QD solutions used varied from 80 s to 20 min. A myoglobin concentration of 25 ng/mL in 100% BCS was used, and four identical QD assembly cycles were performed for each experimental set. At longer incubation times, the QD FI rapidly increased and plateaued (Figure 3a). At a QD concentration of 0.5 μM (the concentration used for the myoglobin assays), half of the final FI level was achieved after 80 s, and the FI reached 90% of the final in 2.5 min. A 5 min QD incubation time was used for the myoglobin assay experiments, which yields a FI greater than 99.9% of the final level. This long incubation time may have been optimal for the LOD achieved with limited cycles of QD amplification; however, shorter QD incubation times can be used for more rapid operations. The total operation time, which is a combination of the number of QD assembly cycles and the incubation time for each QD treatment, can be optimized by varying these conditions. For example, an operation with six assembly cycles and an 80 s incubation time resulted in the signal almost equivalent to an operation with four assembly cycles and a 5 min incubation time, but in about half the total time. This result suggests that our QD amplification method can reach the same LOD as conventional ELISA within 20 min after the sample incubation. Higher FI levels were observed at higher (z)-SA−QD/(z)-B−QD concentrations. Each (z)-SA−QD and (z)-B−QD incubation step was fitted to a first-order Langmuir adsorption model. The specific binding equilibrium constant, *K*, is defined by eq 1

$$K = \frac{\theta}{(1-\theta)[\mathrm{QD}]} \quad (1)$$

where [QD] is the concentration of the QD conjugate and θ is the coverage of the available specific binding sites. The final plateau level of the FI directly reflects the coverage of specifically bound QD conjugate sites. *K* was determined as 2.54 $\times$ 10^6 M^{-1} (see SI, Figure S11 for Langmuir fit). Similar experiments by Demir *et al.* revealed that the specific binding equilibrium constant of commercial SA−QD conjugates on a biotinylated silica surface was 8.43 $\times$ 10^4 M^{-1}, which is more than an order of magnitude lower than ours.[39] This discrepancy is a clear advantage of our QD assembly-based signal amplification technique. The larger equilibrium constant is thought to originate from the zwitterionic

QD surface. Our QD conjugates are about half the hydrodynamic size of the commercial QD conjugates, which should allow more rapid diffusion and rotation. The small zwitterionic surface ligands can also minimize the steric hindrance of the interactions between the surface-immobilized SAs and biotins. Our specific binding equilibrium constant approached the value of $\sim 10^7$, which was comparable to the case of free SA onto a biotinylated surface.[40]

Our biological assembly-based QD signal amplification technique exhibits a broad LDR of sample concentrations. To investigate the layer-by-layer deposition of (z)-SA−QD and (z)-B−QD and the multivalency of the QD conjugates, the FI SNR of the QDs was measured *versus* the number of QD assembly cycles (Figure 3b). A myoglobin sample concentration of 25 ng/mL and QD incubation time of 5 min were used. The SNR showed a linear dependence from 4 to 100 cycles, which is expected to continue beyond 100 cycles because no saturation behavior was observed. Starting from the initial biotinylated secondary antibody anchoring layer, only a few QD assembly cycles seem to be necessary to establish a stable base for the layer-by-layer depositions. The SNR became detectable after four QD assembly cycles and grew linearly with repeated assembly steps. The QD FI is directly dependent on the total number of assembled QDs, which was modeled as the sum of a geometric progression with a rate of $m - 1$ (eq 2)

$$\mathrm{FI} = a \times [(m-1)^n - 1]/(m-2) \qquad (2)$$

where m represents the combined effective multivalency (a geometric mean of the effective multivalencies of both (z)-SA−QD and (z)-B−QD), the number n of QD assembly cycles, and a constant related to the initial QD binding sites, a. By fitting this model to the data, an effective multivalency of 2.0 was obtained for (z)-SA−QD and (z)-B−QD self-assembly, which implies that the QDs assemble through two effective arms and consist of linear rather than branching connections. This method of assembly explains the linear dependence of the QD FI on the number of assembly cycles. These experiments were repeated using samples with different myoglobin concentrations, and the QD FI increased linearly with the number of assembly cycles, irrespective of the sample concentration (Figure 3c). The effective multivalency of the QD conjugate was also unaffected by the myoglobin concentration within our data range. This result explains how our QD amplification is robustly linear over a concentration range of 9 orders of magnitude.

As demonstrated by the bead experiments shown in Figure 1, our QD assembly signal amplification method is based on the presence of minimal nonspecific adsorption of (z)-SA−QD and (z)-B−QD. The nonspecific adsorption behavior of QDs was investigated by measuring the FI of the background area and the changes in standard deviation against the number of QD assembly cycles (Figure 3d). The background was incubated using 100% BCS that did not contain any myoglobin, and the rest of the QD assembly procedure was identical to those of the samples. The responses of the FI and standard deviation of the background to the number of amplification cycles were dramatically differently than those of the samples shown in Figure 3c. The QD FIs of the background increased slowly over repeated assembly cycles, whereas the FI of the samples increased linearly and quickly. The standard deviations of the QD FI of the background rapidly increased, whereas the standard deviation of the sample was small and relatively constant. Monte Carlo simulations were performed to understand the changes in the FI and standard deviation of the background with respect to the number of amplification cycles (dotted lines in Figure 3d; see SI for details and schematics in Figure S5). To obtain the nonspecific adsorption equilibrium constant, K_{nsa}, of (z)-SA−QD and (z)-B−QD with the substrate surface, a substrate with one million surface binding sites available for the nonspecific adsorption and desorption of QDs was simulated for each self-assembly dipping step using K_{nsa} to govern the probability. The assembly between (z)-SA−QD and (z)-B−QD was simulated as complete with the multivalency of 2.0, which assumes that the equilibrium constant for the specific binding is sufficiently larger than for the nonspecific adsorption. Nonspecifically adsorbed QDs can bind to other QDs during each amplification step *via* the SA−biotin interactions before leaving the nonspecific binding site. Nonspecific bindings between QD conjugates were neglected because the zwitterionic QDs showed excellent colloidal stability as confirmed by dynamic light scattering experiments, which indicates that no aggregates or agglomerates form. By fitting these simulations to the actual FI and standard deviation data, a K_{nsa} of 66 was obtained, which is approximately 5 orders of magnitude smaller than the equilibrium constant for specific binding. Our (z)-SA−QD and (z)-B−QD conjugates exhibit a large contrast between specific and nonspecific binding, which is the key for successful signal amplification in immunoassays. These experiments and simulations were repeated for QDs with a different surface species, specifically, the (s)-SA−QD and (s)-B−QD conjugate pair. Monte Carlo simulations returned a K_{nsa} for (s)-SA−QD and (s)-B−QD more than 100 times larger than that for (z)-SA−QD and (z)-B−QD (K_{nsa} of 19 for (s)-SA−QDs/(s)-B−QDs, K_{nsa} of 0.18 for (z)-SA−QDs/(z)-B−QDs). According to our previous studies, (s)-QDs also exhibit good colloidal stability over reasonable pH and salt concentration ranges.[33] The (s)-QDs have a much smaller degree of nonspecific adsorption than both commercial QDs and QDs modified with other functional groups, such as carboxylic acids, primary amines, and quaternary amines (data not shown). Nevertheless, the (s)-SA−QD and

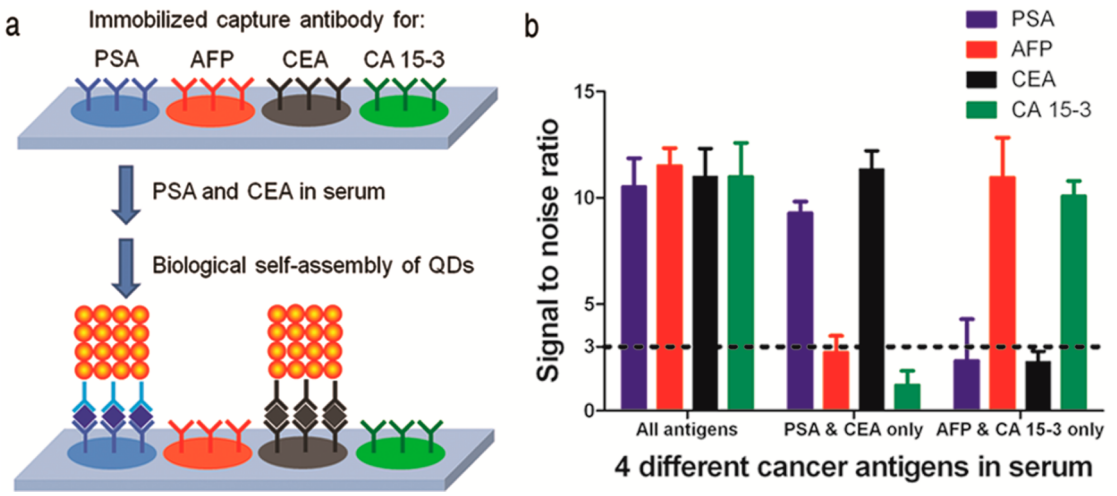

Figure 4. Multiplexed cancer marker immunoassay. (a) Schematic for the multiplexed cancer marker immunoassay that detects prostate-specific antigen and carcinoembryonic antigen through QD self-assembly signal amplification. (b) Bar graph showing the QD fluorescence signal-to-noise ratios for the spots that capture the prostate-specific antigen, α-fetoprotein, carcinoembryonic antigen, and cancer antigen 15−3 cancer markers after 10 QD assembly cycles (represented by blue, red, black, and green bars, respectively). Three cancer marker solutions in 100% bovine calf serum were used; an "all antigens sample" that contained all four cancer markers, a "PSA and CEA only sample" that contained only the prostate-specific antigen and carcinoembryonic antigen and an "AFP and CA 15−3 only sample" that contained only the α-fetoprotein and cancer antigen 15−3. Cancer marker concentrations of 15 ng/mL, 18 ng/mL, 11 ng/mL, and 14 units/mL were used for the prostate-specific antigen, α-fetoprotein, carcinoembryonic antigen, and cancer antigen 15−3, respectively.

(s)-B−QD do not have the property of nonspecific bindings as small as that of the (z)-SA−QD and (z)-B−QD, so only the surface-engineered zwitterionic QD conjugates can be successfully utilized for signal-amplified assays. In our own experiences, polyethylene glycol (PEG)-coated QDs gave a nonspecific adsorption level almost as low as that of our zwitterionic surface QDs. However, the high contrast between specific and nonspecific binding as zwitterionic surfaced QD was difficult to obtain because the bulkiness of the PEGylation might have limited the high specific binding between the SA−biotin motifs.[39]

4-Fold Multiplexed Cancer Marker Immunoassay. We have demonstrated that our QD assembly signal amplification can lower the LOD to tens of copies per milliliter. This reduction in the LOD can be particularly important for the detection of cancer markers. For example, prostate-specific antigen detection on the level of tens of copies can greatly help identify disease relapse during the early stages after surgical treatment.[41] The widespread use of cancer markers in healthcare will ultimately require the rapid, sensitive, and multiplexed detection of many markers at once. Multiplexed ELISA has been fiercely studied, but multiplexed and high-throughput immunoassays are still highly sought after.[42] Multiplexed immunoassay with time-resolved Förster resonance energy transfer (FRET)-based QD biosensor has been reported.[43,44] Subnanomolar sensitive cancer marker immunoassay using a FRET-based QD biosensor has been also investigated.[45,46] Our QD assembly signal amplification technique initiates from a secondary antibody specific to the F_c region of the sandwiched antibodies. Signals from different antigen capture sites that have been precoordinated using the microspot microarray method can be simultaneously amplified and read in a parallel fashion. In addition, our amplification method is not affected by the diffusion or migration of the probes and can, therefore, potentially enable highly miniaturized, integrated, and multiplexed immunoassays "testing all in a single droplet of the test fluid". As a proof-of-concept experiment, a QD assembly signal-amplified multiplexed immunoassay was performed for four cancer markers, prostate-specific antigen (PSA), α-fetoprotein (AFP), carcinoembryonic antigen (CEA), and cancer antigen 15−3 (CA 15−3). Slides with four spots, each at a different immobilized antibody designed to capture one of the four cancer markers, were prepared (Figure 4a). Three samples in 100% BCS were tested. The first sample contained all four cancer markers: PSA (15 ng/mL), AFP (18 ng/mL), CEA (11 ng/mL), and CA 15−3 (14 units/mL). The second sample contained only two cancer markers: PSA and CEA. The final sample contained the other two cancer markers: AFP and CA 15−3. The concentration of each cancer marker was the same in all samples in which they were contained. The used marker concentrations closely matched the known detection limit of conventional ELISA. Other than the test slide and cancer marker samples, all of the experimental procedures were identical to those in the myoglobin assay experiment. QD assembly signal amplification meaningfully enhanced the SNRs after only 10 cycles with a 10 min QD incubation time per cycle. The first sample tested positive for all four cancer markers, the second tested positive only for PSA and CEA, and the last tested positive for only AFP and CA 15−3 (Figure 4b and Figure S6 for raw data). The SNRs

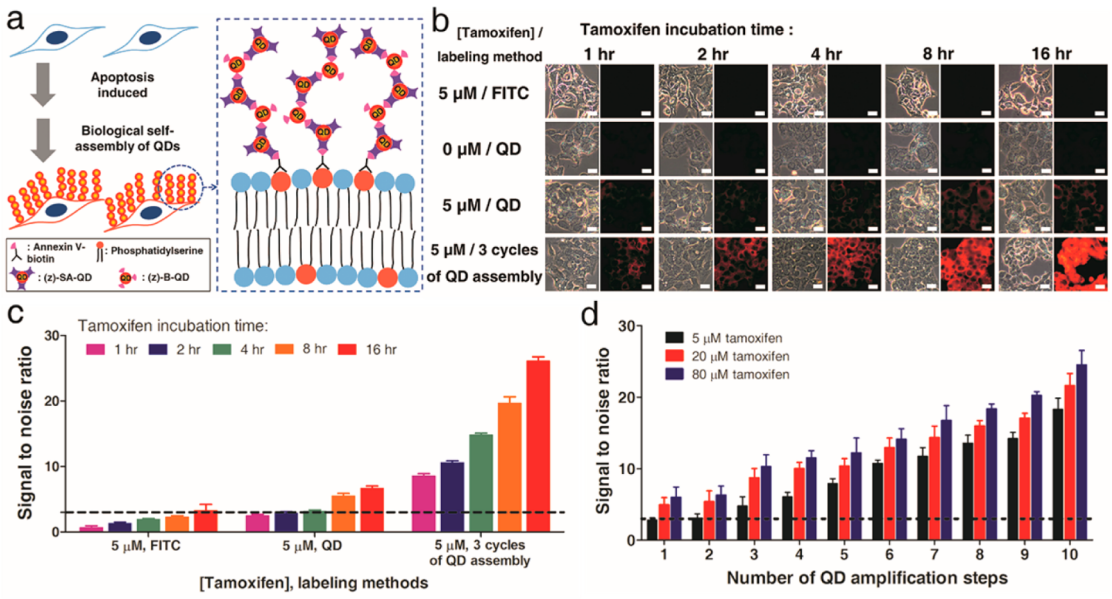

Figure 5. Apoptotic cell imaging and detection. (a) Schematic for the apoptotic cell detection that exploits the QD self-assembly signal amplification from the binding of annexin V–biotins onto phosphatidylserines. (b) Transmission and fluorescence microscope images of HepG2 cells which have been treated by 5 μM of tamoxifen for 1, 2, 4, 8, and 16 h. "FITC", "QD", and "3 cycles of QD assembly", respectively, represent the cells labeled by annexin V–FITC, annexin V–QD, and annexin V–biotin and subsequent three cycles of QD assembly. The control cells with no tamoxifen treatment were also labeled by annexin V–QD (0 μM/QD) (scale bar: 20 μm). (c) Bar graph showing the QD fluorescence signal-to-noise ratios for the apoptotic HepG2 cells shown in (b), where the tamoxifen incubation times of 1, 2, 4, 8, and 16 h are represented by purple, blue, green, orange, and red bars, respectively. (d) Bar graph showing the QD fluorescence signal-to-noise ratios after up to 10 signal amplification steps for the apoptotic HepG2 cells which have been treated by 5, 20, and 80 μM tamoxifen for 4 h (represented by black, red, and blue bars, respectively).

of the positive spots were consistently more than 3 times higher than for the negative spots which yielded SNRs less than 3. However, they have a slight chance of false positive errors because the assembly cycles of only 10 were performed. As shown in Figure 3, the false positive error can be insignificant as increasing the number of QD assembly cycles. The false positive is presumably due to the nonspecific adsorption of biotinylated secondary antibodies onto the substrate. The false positive adsorption can dissociate in a random fashion as assembly cycles continue. Our QD assembly signal amplification method has been successfully used for the multiplexed immunoassay of four different cancer markers in the complex medium of 100% BCS without noticeable cross-reactivity.

Apoptotic Cell Imaging and Detection. Signal amplification by our layer-by-layer biological self-assembly of QDs has been utilized for sensitive and multiplexed immunoassays. To demonstrate that our QD signal amplification can be a universal platform for a variety of applications of sensing and imaging, it was further applied for sensitive and early detection and imaging of apoptotic cells. Sensitive and early detection of apoptosis can allow rapid screening and discovery of potential targets for therapeutic treatments for disease such as cancer that are related to the imbalance between cell proliferation and loss.[47] At the early stage of apoptosis, redistributions of phospholipids between the inner and the outer membranes begin. As a hallmark for apoptosis, externalization of phosphatidylserine (PS) is typically detected by annexin V.[48] For example, photostable apoptosis imaging using annexin V–QD conjugates have been reported by van den Berg *et al.*[49] We adopted the annexin V-affinity-based assays for our signal amplification assembly method (see SI for details). Human hepatocellular carcinomas, HepG2 cells, were induced to apoptosis by tamoxifen, without prior enrichment or purification steps. For the signal amplification, the apoptotic HepG2 cells were treated by annexin V–biotin conjugates and were subsequently treated by (z)-SA–QD and (z)-B–QD conjugates to achieve the layer-by-layer QD assembly (Figure 5a). Tamoxifen (5 μM) was treated to the cells, and the apoptosis was imaged using an annexin V–FITC conjugate, annexin V–QD conjugate, or three cycles of our QD assembly method after the coincubation for 1, 2, 4, 8, and 16 h (Figure 5b). We have also performed a control experiment with identical (z)-SA–QD and (z)-B–QD assemblies without the treatment of annexin V–biotin. For the control case without annexin V–biotin treatment, the signal was more than 590 times smaller than the counterpart (see SI, Figure S12). FITC failed to show any apoptotic cells with the images similar to the control 0 μM/QD. The conventional QD conjugate has only marginally visualized the apoptotic cells. The sample treated by QD assembly showed the progression of apoptosis over time with remarkable sensitivity. The three cycles of QD assembly, which took only 30 min, have visualized the apoptotic cells at as early as 1 h after the tamoxifen

treatment. To quantify the enhancement by signal amplification using QD assembly, SNRs of the images in Figure 5b were compared (Figure 5c; see SI for the SNR evaluation protocols and Figure S8a for the raw data). The increase in SNR over time was found throughout all the labeling methods; however, all the FITC cases and conventional QD cases before 8 h did not exceed the SNR of 3. The QD assembly signal amplification has consistently multiplied the SNRs by more than 3 times those of conventional QD cases, which resulted in the early detection and sensitive imaging of the apoptosis progression. The dose of 5 μM tamoxifen was judiciously chosen because the dosage has been reported to be too low to reveal the apoptosis of HepG2 cells even by caspase assays that detect mitochondrial change which precedes the membrane change.[50] Our results showed the detection of early apoptosis that is more sensitive than the caspase assay. For the annexin V–FITC apoptosis assay, an order of magnitude larger tamoxifen dosage was required for the positive results (Figure S9). To demonstrate the large dynamic range and robustness of our QD assembly signal amplification method, the cases of different tamoxifen doses were monitored as increasing the assembly steps up 10 (Figure 5d and Figure S8b for the raw data). Tamoxifen-treated HepG2 cells (5, 20, and 80 μM) were incubated for 4 h, and the SNRs for the fluorescence images of apoptotic cells were obtained. As is similar to the immunoassay cases, the SNRs increased linearly by the repeated incubation steps, which suggests layer-by-layer assembly of QDs from PSs of the apoptotic cell membranes.

CONCLUSIONS

To summarize, we report a new, fluorescence-based, heterogeneous immunoassay method with subattomolar sensitivity, an LOD of tens of copies per milliliter, an LDR for concentration of over 9 orders of magnitude, and high multiplexing power, which allows for a highly miniaturized and integrated sensing platform. Immuno-captured target molecules were transduced into specific binding of QDs, and then the fluorescence signal was amplified through the layer-by-layer assembly of an SA/biotin QD conjugate pair. This signal amplification was accomplished through a simple, alternating dipping process and was efficient enough to reach conventional ELISA detection levels in half the time ELISA requires. Alternatively, subattomolar sensitivity could be achieved by repeated signal amplification over a reasonable length of time. This rapid, selective, and sensitive signal amplification technique relied on the high contrast between the specific and nonspecific binding equilibria of the engineered zwitterionic surface of (z)-SA–QD and (z)-B–QD. Kinetic studies gave a specific to nonspecific binding equilibrium constant ratio of approximately 5 orders of magnitude. The small zwitterionic surface ligand provides a specific binding affinity of (z)-SA–QD to (z)-B–QD approaching that of free SA to a biotinylated surface. The minimal amount of nonspecific adsorption of the (z)-QDs critically enhanced the SNR of the layer-by-layer assembly immunoassays. Our signal amplification method can be easily applied to other antigenic targets and potentially to other systems using many host–guest interactions. To demonstrate the applicability of our signal amplification, sensitive imaging and early detection of apoptotic cells were showcased. We hope that the high sensitivity and multiplexing power of this signal amplification can be used for the parallel analysis of proteins or lipids with small copy numbers, for example, at a single cell level.

EXPERIMENTAL SECTION

QD Biological Self-Assemblies onto Biotinylated Agar Beads. Biotinylated agar beads (diameter = ~100 μm) were dispersed in 200 μL of (z)-SA–QD conjugate solution (500 nM). The beads were coincubated with the QD conjugate for 5 min. To remove excess QD conjugates and to collect the beads, the mixture solution was filtered using fritted funnel and washed with excess DI water. Small aliquot of the beads was collected and placed on a glass substrate to image the fluorescence by a fluorescence microscope equipped with a CCD camera (1 incubation step in Figure 1c). Remaining beads were dispersed in 200 μL of (z)-B–QD conjugate solution (500 nM). The beads were coincubated with the QD conjugate for 5 min. After an identical collection and washing step as used for step 1, fluorescence microscope image of an aliquot was taken (2 incubation steps in Figure 1c). The coincubations with either (z)-SA–QD or (z)-B–QD were alternated for following incubation steps to 10. QD biological self-assembly was performed in an identical manner for (s)-SA–QD/(s)-B–QD pair and for the unconjugated physical mixture pair.

Myoglobin Immunoassay Using QD Signal Amplification by Biological Self-Assembly of (z)-SA–QD/(z)-B–QD Pairs. Various concentrations of myoglobin solution were incubated on each myoglobin antibody (Ab)-immobilized substrates as follows: 0.98 ag/mL, 9.8 ag/mL, 98 ag/mL, 0.98 fg/mL, 9.8 fg/mL, 98 fg/mL, 0.98 pg/mL, 9.8 pg/mL, 98 pg/mL, 390 pg/mL, 1.6 ng/mL, 6.3 ng/mL, 25 ng/mL, 0.10 μg/mL, and 0.40 μg/mL of myoglobin solution in 100% bovine calf serum (BCS) or PBS buffer (50 mM, pH 7.5). The substrates were washed by excess DI water, and 30 μL of mouse monoclonal Ab to human myoglobin (5.5 nM in PBS) was incubated onto the substrate for 30 min. The substrates were again washed by excess DI water, and 30 μL of goat polyclonal biotinylated Ab to mouse IgG (6 nM in PBS) was incubated with the substrate for 30 min. The substrates were washed by excess DI water. (z)-SA–QD and (z)-B–QD conjugates were alternatively treated to assemble QDs by layer-by-layer beginning from the biotinylated secondary antibodies. Using a mechanized dipper, the substrates were first dipped into a (z)-SA–QD solution (0.50 μM in PBS) for 5 min, rinsed by dipping in a DI water bath for 20 s, then submerged in a (z)-B–QD solution (0.50 μM in PBS) for 5 min. One cycle of QD deposition was completed by another rinsing step in DI water bath. Different QD assembly cycles of 5, 10, 20, 50, and 100 were performed, and the signal-to-noise ratios (SNRs) of the fluorescence signal were obtained by using a fluorescence microscope equipped with a CCD camera. The SNR is defined as the difference

between the FI from myoglobin samples and that from the background (identical substrates without myoglobin) divided by the standard deviation of the background FI.

Adsorption Kinetics Studies for QD Biological Self-Assembly by (z)-SA−QD/(z)-B−QD Pairs. Thirty microliters of myoglobin solution (25 ng/mL in 100% BCS) was incubated on myoglobin Ab-immobilized substrates for 30 min. The substrate was washed by excess DI water, and 30 μL of mouse monoclonal Ab to human myoglobin (5.5 nM in PBS) was incubated onto the substrates for 30 min. The substrate was again washed by excess DI water, and 30 μL of goat polyclonal biotinylated Ab to mouse IgG (6 nM in PBS) was incubated on the substrate for 30 min. The substrate was washed by excess DI water. Then, 30 μL of (z)-SA−QD conjugate solution (0.05, 0.5, or 5 μM in PBS) was incubated on the substrate for various incubation times of 0, 80, 180, 320, 600, or 1200 s. To remove unbound QD conjugates, the substrate was washed by excess DI water, and 30 μL of (z)-B−QD conjugate solution (0.05, 0.5, or 5 μM in PBS) was incubated by the similar fashion as that of (z)-SA−QD. One cycle of QD assembly was completed by another washing with excess DI water. Many cycles of QD assembly were repeated. Fluorescent images of the myoglobin-captured substrate were taken by using a fluorescence microscope equipped with a CCD camera.

Calculation of Specific Binding Equilibrium Constant (K) for QD Self-Assembly. From Figure 2a results, the specific binding equilibrium constant, K, was calculated as follows.

$$[\mathrm{QD}] + [\mathrm{site}_0] \leftrightarrow [\mathrm{QD}\cdot\mathrm{site}]$$

where $[\mathrm{site}_0]$ is the number of available total binding sites of the substrate and $[\mathrm{QD}\cdot\mathrm{site}]$ is the number of the QD-bound sites of the substrate.

Rate of specific adsorption of QDs, v_{ad}

$$v_{ad} = k_{ad}\cdot[\mathrm{QD}]\cdot(1-\theta)\cdot\sigma_0$$

Rate of desorption of QDs, v_d

$$v_d = k_d\cdot\theta\cdot\sigma_0$$

$$K = \frac{k_{ad}}{k_d} = \frac{\theta}{1-\theta}\cdot\frac{1}{[\mathrm{QD}]}$$

where θ is a coverage of the total binding site, k_{ad} is the rate constant of specific adsorption of QDs, k_d is the rate constant for QD desorption, and σ_0 is the concentration of the binding sites (m^{-2}).

Monte Carlo Simulation Studies for Nonspecific Adsorption Equilibrium. The nonspecific adsorption equilibrium constant, K_{nsa}, was calculated as follows.

$$[\mathrm{QD}] + [\mathrm{site}_0'] \leftrightarrow [\mathrm{QD}\cdot\mathrm{site}']$$

where $[\mathrm{site}_0']$ is the number of available total nonspecific adsorption sites of the substrate and $[\mathrm{QD}\cdot\mathrm{site}']$ is the number of nonspecifically adsorbed sites of the substrate.

Rate of nonspecific adsorption of QDs, v_{ad}'

$$v_{ad}' = k_{ad}'\cdot(1-\theta')\cdot\sigma_0'$$

Rate of desorption of QDs from the substrate, v_d'

$$v_d' = k_d'\cdot\theta\cdot\sigma_0'$$

$$K_{nsa} = \frac{k_{ad}'}{k_d'} = \frac{\theta'}{1-\theta'}$$

where θ' is the coverage of the total substrate site, k_{ad}' is the rate constant for nonspecific adsorption of QDs, k_d' is the rate constant of QD desorption, and σ_0' is the concentration of the surface site (m^{-2}) which was set as 10^6 for the simulation; θ' governs the probability whether (z)-SA−QD or (z)-B−QD adsorb onto or desorb from the substrate. The assembly between (z)-SA−QD and (z)-B−QD was simulated as complete with their multivalency of 2.0. The number of QD assembly cycles was 100.

4-Fold Multiplexed Cancer Marker Immunoassay. Three samples were tested; first sample containing all four cancer markers of PSA (15 ng/mL), AFP (18 ng/mL), CEA (11 ng/mL), and CA 15−3 (14 unit/mL), second sample containing only two cancer markers of PSA and CEA, and last sample containing the other two cancer markers AFP and CA 15−3. The substrate was spotted by PSA, AFP, CEA, and CA 15−3 antibodies in precoordinated positions. For each cancer marker serum sample solution, 30 μL of the sample solution was incubated on the substrate for 30 min. To remove excess antigens, the substrate was washed with excess DI water. After the washing step, the substrate was dipped into the detection Ab cocktail solution which contains PSA, AFP, CEA and CA 15−3 Ab (5.5 nM for each Ab) for 30 min. To remove excess Abs, the substrate was washed with excess DI water. The substrate was dipped into the biotinylated anti-IgG antibody solution (6 nM) for 30 min. To remove excess Abs, the substrate was washed with excess DI water. The substrate was dipped into (z)-SA−QDs solution (10 mL, 500 nM) for 5 min. To remove excess QD conjugates, each substrate was washed by excess DI water for 20 s. The substrate was subsequently dipped into (z)-B−QDs (10 mL, 500 nM) for 5 min. Another rinsing step in the DI water bath completed one QD deposition cycle. Ten cycles of QD assembly was performed using a mechanized dipper. After the 10 cycles of QD assembly, PL microscope images of the substrate were taken using a fluorescence microscope equipped with a CCD camera. The SNR is defined as the difference between the FI from the substrate with cancer markers and that from the background (identical substrates without cancer markers) divided by the standard deviation of the background FI.

Apoptotic Cell Imaging and Detection Using a QD Signal Amplification Method. HepG2 cells, human liver hepatocellular carcinoma cell line, were cultured in each well of multiwell slide glass. The cultured HepG2 cells were treated with tamoxifen solutions which were prepared to have the concentrations of 5, 20, and 80 μM for 4 h. These tamoxifen solutions were prepared in MEM serum-free culture medium. The control sample, which was treated pure serum-free media, was used as the background signal. After the treatments, cells were washed with PBS buffer and treated with annexin V−biotin conjugates (0.7 μM) in binding buffer (10 mM HEPES, 140 mM NaCl, 2.5 mM $CaCl_2$, pH 7.4) for 15 min at room temperature. After the treatments, cells were washed with PBS buffer and fixed cells with 4% formaldehyde solution. After the treatments, cells were washed with PBS buffer and incubated with 3% bovine serum albumin (BSA) for 30 min. To remove excess BSA, the cell-attached substrate was washed with excess DI water. The cell-attached substrate was dipped into (z)-SA−QDs solution (10 mL, 500 nM) for 5 min. To remove excess QD conjugates, the cell-attached substrate was washed with excess DI water for 20 s. The cell-attached substrate was subsequently dipped into (z)-B−QDs (10 mL, 500 nM) for 5 min. Another rinsing step in the DI water bath completed one QD deposition cycle. Five cycles of QD assembly was performed. After the five cycles of QD assembly, PL microscope images of the cells were taken using a fluorescence microscope equipped with a CCD camera. For early apoptosis diagnosis experiments, the cultured HepG2 cells were treated with tamoxifen solutions which were prepared to have the concentrations of 5 μM for 1, 2, 4, 8, and 16 h. These tamoxifen solutions were prepared in MEM serum-free culture medium. The control sample, which was treated pure serum-free media, was used as the background signal. After the treatments, annexin V−biotin and QD self-assembly methods were the same as mentioned above. For "QD" samples, annexin V−biotin and (z)-SA−QDs were subsequently used for labeling. For "3 cycles of QD assembly" samples, three cycles of QD biological self-assembly was performed as mentioned above. PL microscope images of the cells were taken using a fluorescence microscope equipped with a CCD camera. The SNR is defined as the difference between the FI from tamoxifen-treated cells and that from the background (identical cells without tamoxifen) divided by the standard deviation of the background FI.

Optical Detection Setup. The fluorescent images were taken using Zeiss Axiocam HR CCD camera. Photos of all samples have

been taken with 12 different parts of the substrate, and their signal and standard deviation have been measured and processed by the Photoshop program.

Conflict of Interest: The authors declare no competing financial interest.

Acknowledgment. This work was supported by the Korea Health Technology R&D Project, Ministry of Health & Welfare (A121763), the Priority Research Center Program through NRF 2009-0094036, and NRF funded by the Ministry of Education, Science and Technology (2011-0019635).

Supporting Information Available: Details of experimental procedures, absorption spectrum and photoluminescence spectrum of QDs and QD conjugates, hydrodynamic size measurements of QD conjugates and its mixture, bar graph of QD fluorescence intensities *vs* myoglobin concentrations in 100% bovine calf serum, signal-to-noise ratio *vs* myoglobin concentrations in 100% bovine calf serum and buffer, schematic representation of the nonspecific adsorption and desorption of QD conjugates self-assembly, bar graph showing the QD fluorescence intensities for multiplexed cancer marker immunoassay, bar graph showing the conventional myoglobin ELISA results, bar graph showing the QD fluorescence intensities for the apoptotic HepG2 cells, conventional annexin V−FITC apoptotic cell assay results, plots of the fluorescence intensities of QD conjugates *vs* myoglobin concentrations after 100 cycles of QD assembly with regression graph, Langmuir fitting of adsorption kinetics data, and additional fluorescence and transmission microscope images of control (without annexin V−biotin) and sample (without annexin V−biotin) of apoptotic cell imaging experiment. This material is available free of charge *via* the Internet at http://pubs.acs.org.

REFERENCES AND NOTES

1. Green, E. D.; Guyer, M. S. Charting a Course for Genomic Medicine from Base Pairs to Bedside. *Nature* **2011**, *470*, 204–213.
2. Wulfkuhle, J. D.; Liotta, L. A.; Petricoin, E. F. Proteomic Applications for the Early Detection of Cancer. *Nat. Rev. Cancer* **2003**, *3*, 267–275.
3. Considine, R. V.; Sinha, M. K.; Heiman, M. L.; Kriauciunas, A.; Stephens, T. W.; Nyce, M. R.; Ohannesian, J. P.; Marco, C. C.; McKee, L. J.; Bauer, T. L.; *et al.* Serum Immunoreactive-Leptin Concentrations in Normal-Weight and Obese Humans. *N. Engl. J. Med.* **1996**, *334*, 292–295.
4. Hemmila, I. Fluoroimmunoassays and Immunofluorometric Assays. *Clin. Chem.* **1985**, *31*, 359–370.
5. Wild, D. *The Immunoassay Handbook*, 3rd ed.; Elsevier: Kidlington, UK, 2005.
6. Giljohann, D. A.; Mirkin, C. A. Drivers of Biodiagnostic Development. *Nature* **2009**, *462*, 461–464.
7. Park, S.-J.; Taton, T. A.; Mirkin, C. A. Array-Based Electrical Detection of DNA with Nanoparticle Probes. *Science* **2002**, *295*, 1503–1506.
8. Qu, W.; Liu, Y.; Liu, D.; Wang, Z.; Jiang, X. Copper-Mediated Amplification Allows Readout of Immunoassays by the Naked Eye. *Angew. Chem., Int. Ed.* **2011**, *50*, 3442–3445.
9. Sano, T.; Smith, C.; Cantor, C. Immuno-PCR: Very Sensitive Antigen Detection by Means of Specific Antibody-DNA Conjugates. *Science* **1992**, *258*, 120–122.
10. Wang, J.; Liu, G.; Munge, B.; Lin, L.; Zhu, Q. DNA-Based Amplified Bioelectronic Detection and Coding of Proteins. *Angew. Chem., Int. Ed.* **2004**, *43*, 2158–2161.
11. Mason, J. T.; Xu, L.; Sheng, Z.-m.; O'Leary, T. J. A Liposome-PCR Assay for the Ultrasensitive Detection of Biological Toxins. *Nat. Biotechnol.* **2006**, *24*, 555–557.
12. Das, J.; Aziz, M. A.; Yang, H. A Nanocatalyst-Based Assay for Proteins: DNA-Free Ultrasensitive Electrochemical Detection Using Catalytic Reduction of *p*-Nitrophenol by Gold-Nanoparticle Labels. *J. Am. Chem. Soc.* **2006**, *128*, 16022–16023.
13. Nam, J.-M.; Thaxton, C. S.; Mirkin, C. A. Nanoparticle-Based Bio-Bar Codes for the Ultrasensitive Detection of Proteins. *Science* **2003**, *301*, 1884–1886.
14. Exley, D.; Ekeke, G. I. Fluoroimmunoassay of 5[α]-dihydrotestosterone. *J. Steroid Biochem.* **1981**, *14*, 1297–1302.
15. Alivisatos, P. The Use of Nanocrystals in Biological Detection. *Nat. Biotechnol.* **2004**, *22*, 47–52.
16. Wu, X.; Liu, H.; Liu, J.; Haley, K. N.; Treadway, J. A.; Larson, J. P.; Ge, N.; Peale, F.; Bruchez, M. P. Immunofluorescent Labeling of Cancer Marker Her2 and Other Cellular Targets with Semiconductor Quantum Dots. *Nat. Biotechnol.* **2003**, *21*, 41–46.
17. Chan, W. C. W.; Maxwell, D. J.; Gao, X.; Bailey, R. E.; Han, M.; Nie, S. Luminescent Quantum Dots for Multiplexed Biological Detection and Imaging. *Curr. Opin. Biotechnol.* **2002**, *13*, 40–46.
18. Medintz, I. L.; Uyeda, H. T.; Goldman, E. R.; Mattoussi, H. Quantum Dot Bioconjugates for Imaging, Labelling and Sensing. *Nat. Mater.* **2005**, *4*, 435–446.
19. Goldman, E.; Medintz, I.; Mattoussi, H. Luminescent Quantum Dots in Immunoassays. *Anal. Bioanal. Chem.* **2006**, *384*, 560–563.
20. Bhang, S. H.; Won, N.; Lee, T.-J.; Jin, H.; Nam, J.; Park, J.; Chung, H.; Park, H.-S.; Sung, Y.-E.; Hahn, S. K.; *et al.* Hyaluronic Acid−Quantum Dot Conjugates for *In Vivo* Lymphatic Vessel Imaging. *ACS Nano* **2009**, *3*, 1389–1398.
21. McLaurin, E. J.; Greytak, A. B.; Bawendi, M. G.; Nocera, D. G. Two-Photon Absorbing Nanocrystal Sensors for Ratiometric Detection of Oxygen. *J. Am. Chem. Soc.* **2009**, *131*, 12994–13001.
22. Snee, P. T.; Somers, R. C.; Nair, G.; Zimmer, J. P.; Bawendi, M. G.; Nocera, D. G. A Ratiometric CdSe/ZnS Nanocrystal pH Sensor. *J. Am. Chem. Soc.* **2006**, *128*, 13320–13321.
23. Kim, S.; Lim, Y. T.; Soltesz, E. G.; De Grand, A. M.; Lee, J.; Nakayama, A.; Parker, J. A.; Mihaljevic, T.; Laurence, R. G.; Dor, D. M.; *et al.* Near-Infrared Fluorescent Type II Quantum Dots for Sentinel Lymph Node Mapping. *Nat. Biotechnol.* **2004**, *22*, 93–97.
24. Wu, Y.; Chakrabortty, S.; Gropeanu, R. A.; Wilhelmi, J.; Xu, Y.; Er, K. S.; Kuan, S. L.; Koynov, K.; Chan, Y.; Weil, T. pH-Responsive Quantum Dots *via* an Albumin Polymer Surface Coating. *J. Am. Chem. Soc.* **2010**, *132*, 5012–5014.
25. Weiyong, M.; Jia, G.; Wuli, Y.; Changchun, W.; Jia, H.; Jiyao, C. Synthesis of High-Quality Near-Infrared-Emitting CdTeS Alloyed Quantum Dots *via* the Hydrothermal Method. *Nanotechnology* **2007**, *18*, 485611.
26. Soman, C. P.; Giorgio, T. D. Quantum Dot Self-Assembly for Protein Detection with Sub-picomolar Sensitivity. *Langmuir* **2008**, *24*, 4399–4404.
27. Soman, C. P.; Giorgio, T. D. Sensitive and Multiplexed Detection of Proteomic Antigens *via* Quantum Dot Aggregation. *Nanomed. Nanotechnol. Biol. Med.* **2009**, *5*, 402–409.
28. Kim, D.; Daniel, W. L.; Mirkin, C. A. Microarray-Based Multiplexed Scanometric Immunoassay for Protein Cancer Markers Using Gold Nanoparticle Probes. *Anal. Chem.* **2009**, *81*, 9183–9187.
29. Park, J.; Nam, J.; Won, N.; Jin, H.; Jung, S.; Jung, S.; Cho, S.-H.; Kim, S. Compact and Stable Quantum Dots with Positive, Negative, or Zwitterionic Surface: Specific Cell Interactions and Non-specific Adsorptions by the Surface Charges. *Adv. Funct. Mater.* **2011**, *21*, 1558–1566.
30. Muro, E.; Pons, T.; Lequeux, N.; Fragola, A.; Sanson, N.; Lenkei, Z.; Dubertret, B. Small and Stable Sulfobetaine Zwitterionic Quantum Dots for Functional Live-Cell Imaging. *J. Am. Chem. Soc.* **2010**, *132*, 4556–4557.
31. Susumu, K.; Oh, E.; Delehanty, J. B.; Blanco-Canosa, J. B.; Johnson, B. J.; Jain, V.; Hervey, W. J.; Algar, W. R.; Boeneman, K.; Dawson, P. E.; *et al.* Multifunctional Compact Zwitterionic Ligands for Preparing Robust Biocompatible Semiconductor Quantum Dots and Gold Nanoparticles. *J. Am. Chem. Soc.* **2011**, *133*, 9480–9496.
32. Choi, H. S.; Liu, W.; Misra, P.; Tanaka, E.; Zimmer, J. P.; Itty Ipe, B.; Bawendi, M. G.; Frangioni, J. V. Renal Clearance of Quantum Dots. *Nat. Biotechnol.* **2007**, *25*, 1165–1170.
33. Jin, H.; Nam, J.; Park, J.; Jung, S.; Im, K.; Hur, J.; Park, J.-J.; Kim, J.-M.; Kim, S. Strong Polyelectrolyte Quantum Dot Surface

for Stable Bioconjugation and Layer-by-Layer Assembly Applications. *Chem. Commun.* **2011**, *47*, 1758–1760.
34. Rauf, S.; Glidle, A.; Cooper, J. M. Production of Quantum Dot Barcodes Using Biological Self-Assembly. *Adv. Mater.* **2009**, *21*, 4020–4024.
35. Witherspoon, L. R.; Shuler, S. E.; Garcia, M. M.; Zollinger, L. A. Assessment of Serum Myoglobin as a Marker for Acute Myocardial Infarction. *J. Nucl. Med.* **1979**, *20*, 115–119.
36. MacDougall, D.; Crummett, W. B. Guidelines for Data Acquisition and Data Quality Evaluation in Environmental Chemistry. *Anal. Chem.* **1980**, *52*, 2242–2249.
37. Gul, O.; Calay, E.; Sezerman, U.; Basaga, H.; Gurbuz, Y. Sandwich-Type, Antibody Microarrays for the Detection and Quantification of Cardiovascular Risk Markers. *Sens. Actuators, B* **2007**, *125*, 581–588.
38. Dyke, K. V.; Dyke, C. V.; Woodfork, K. *Luminescence Biotechnology*; CRC Press: New York, 2002.
39. Seker, U. O. S.; Zengin, G.; Tamerler, C.; Sarikaya, M.; Demir, H. V. Assembly Kinetics of Nanocrystals *via* Peptide Hybridization. *Langmuir* **2011**, *27*, 4867–4872.
40. Zhao, S.; Walker, D. S.; Reichert, W. M. Cooperativity in the Binding of Avidin to Biotin-Lipid-Doped Langmuir–Blodgett Films. *Langmuir* **1993**, *9*, 3166–3173.
41. Yu, H.; Diamandis, E.; Prestigiacomo, A.; Stamey, T. Ultrasensitive Assay of Prostate-Specific Antigen Used for Early Detection of Prostate Cancer Relapse and Estimation of Tumor-Doubling Time after Radical Prostatectomy. *Clin. Chem.* **1995**, *41*, 430–434.
42. Wiese, R.; Belosludtsev, Y.; Powdrill, T.; Thompson, P.; Hogan, M. Simultaneous Multianalyte ELISA Performed on a Microarray Platform. *Clin. Chem.* **2001**, *47*, 1451–1457.
43. Geißler, D.; Charbonniére, L. J.; Ziessel, R. F.; Butlin, N. G.; Löhmannsröben, H.-G.; Hildebrandt, N. Quantum Dot Biosensors for Ultrasensitive Multiplexed Diagnostics. *Angew. Chem., Int. Ed.* **2010**, *49*, 1396–1401.
44. Geißler, D.; Stufler, S.; Löhmannsröben, H.-G.; Hildebrandt, N. Six-Color Time-Resolved Föster Resonance Energy Transfer for Ultrasensitive Multiplexed Biosensing. *J. Am. Chem. Soc.* **2013**, *135*, 1102–1109.
45. Wegner, K. D.; Jin, Z.; Lindén, S.; Jennings, T. L.; Hildebrandt, N. Quantum-Dot-Based Föster Resonance Energy Transfer Immunoassay for Sensitive Clinical Diagnostics of Low-Volume Serum Samples. *ACS Nano* **2013**, *7*, 7411–7419.
46. Chen, M.-J.; Wu, Y.-S.; Lin, G.-F.; Hou, J.-Y.; Li, M.; Liu, T.-C. Quantum-Dot-Based Homogeneous Time-Resolved Fluoroimmunoassay of α-Fetoprotein. *Anal. Chim. Acta* **2012**, *741*, 100–105.
47. Kerr, J. F. R.; Winterford, C. M.; Harmon, B. V. Apoptosis. Its Significance in Cancer and Cancer Therapy. *Cancer* **1995**, *73*, 2013–2026.
48. Van Engeland, M.; Nieland, L. J. W.; Ramaekers, F. C. S.; Schutte, B.; Reutelingsperger, C. P. M. Annexin V-Affinity Assay: A Review on an Apoptosis Detection System Based on Phosphatidylserine Exposure. *Cytometry* **1998**, *31*, 1–9.
49. Le Gac, S.; Vermes, I.; Van den Berg, A. Quantum Dots Based Probes Conjugated to Annexin V for Photostable Apoptosis Detection and Imaging. *Nano Lett.* **2006**, *6*, 1863–1869.
50. Riss, T. L.; Moravec, R. A. Use of Multiple Assay Endpoints To Investigate the Effects of Incubation Time, Dose of Toxin, and Plating Density in Cell-Based Cytotoxicity Assays. *Assay Drug Dev. Tech.* **2004**, *2*, 52–61.